The 69-μm forsterite band as a dust temperature indicator

J. E. Bowey,[1]★ M. J. Barlow,[1] F. J. Molster,[2] A. M. Hofmeister,[3] C. Lee,[4] C. Tucker,[4] T. Lim,[5] P. A. R. Ade[4] and L. B. F. M. Waters[6]

[1]*Department of Physics and Astronomy, University College London, Gower Street, London WC1E 6BT*
[2]*ESTEC/ESA, RSSD-ST, Keplerlaan 1, 2201 AZ Noordwijk, the Netherlands*
[3]*Department of Earth and Planetary Science, Washington University, Box 1169, 1 Brookings Drive, St Louis, MO 63130, USA*
[4]*Department of Physics and Astronomy, University of Wales, Cardiff, 5 The Parade, Cardiff CF24 3YB*
[5]*Space Science Department, Rutherford Appleton Laboratory, Chilton, Didcot OX11 0QX*
[6]*Astronomical Institute, University of Amsterdam, Kruislaan 403, 1098 SJ Amsterdam, the Netherlands*

ABSTRACT

A band of pure crystalline forsterite (100 per cent Mg_2SiO_4) occurs at $69.67\,\mu m$ at room temperature (295 K); for olivines with $\gtrsim 10$ per cent Fe the corresponding feature is at $\gtrsim 73\,\mu m$. The Mg-rich forsterite feature is observed in a variety of *ISO* LWS spectra, but the corresponding Fe-rich olivine feature is not. For the 10 astronomical sources in our sample, the forsterite band peaks in the $68.9–69.3\,\mu m$ range and narrows with decreasing peak wavelength. This is consistent with the shortwards shifting of the peak observed when laboratory samples are cooled to 77 K ($69.07\,\mu m$) and 3.5 K ($68.84\,\mu m$). The shifted peak is produced by lattice contraction and the sharpening is due to a decrease in phonon density at lower temperatures. However, the astronomical bands are narrower than those of the laboratory samples. By comparing the laboratory and astronomical peak wavelengths, we deduce characteristic forsterite 69-μm band temperatures that are in the $27–84\,K$ range for the eight post-main-sequence objects in our sample. These values are shown to be consistent with the local continuum temperatures derived using a $\beta = 1.5$ dust emissivity index, similar to derived interstellar values of the opacity index. For the pre-main sequence-objects HD 100546 and MWC 922, the characteristic 69-μm forsterite band temperatures (127 ± 18 and $139 \pm 10\,K$, respectively) are significantly higher than those of the post-main-sequence objects and are more than twice as high as their local continuum temperatures deduced using $\beta = 1.5$. The assumption of large grains ($\beta = 0$) can produce agreement between the derived 69-μm and continuum temperatures for one of these objects but not for the other – a spatial separation between the forsterite and continuum-emitting grains may therefore be implied for it. We conclude that observations of the peak wavelength and FWHM of the 69-μm forsterite band show great promise as a new diagnostic of characteristic grain temperatures.

Key words: line: identification – stars: AGB and post-AGB – circumstellar matter – stars: pre-main-sequence – dust, extinction – infrared: general.

1 INTRODUCTION

Forsterite was first identified as an important component of some circumstellar dust environments based on the strength and position of narrow bands at 23.7 and $33.5\,\mu m$ in the *Infrared Space Observatory* (*ISO*) Short Wavelength Spectrometer (SWS) spectrum of the isolated Herbig Ae/Be star HD 100546 (Waelkens et al. 1996). Malfait et al. (1998) later associated a band at $69\,\mu m$ in the Long Wavelength Spectrometer (LWS) spectrum of HD

100546 with forsterite and pointed out that its presence indicated that forsterite was not confined solely to the inner part of the disc. They found that the relative strengths of the forsterite features between 11 and $30\,\mu m$ are correctly described with a temperature of $210 \pm 5\,K$, but cooler particles $(40–55\,K)$ were required to account for the longer wavelength features. They noted that this band could be the best discriminant for the Mg/Fe ratio since it occurs at $69.67\,\mu m$ for pure forsterite (Bowey et al. 2001, hereafter Paper I) and at $73\,\mu m$ or more for mixtures with more than 10 per cent iron (Koike, Shibai & Tuchiyama 1993). In fayalite, Fe_2SiO_4, the nearest room-temperature band occurs at $94\,\mu m$ (Hofmeister

★E-mail: jeb@star.ucl.ac.uk

1997). However, the composition of the grains cannot be solely responsible for the difference between the astronomical and laboratory features, since the observed astronomical features peak between 68.9 and 69.3 µm, 0.8–0.4 µm shortwards of the room-temperature peak for pure forsterite, and are 0.2–0.8 µm wide (FWHM) whilst the laboratory peak has a FWHM of 1.4 µm at room temperature. The smaller FWHM of the astronomical peak might indicate that the grains have a higher purity than the laboratory sample. However, X-ray diffraction analysis of the laboratory samples measured in Paper I showed that the sample was formed of well-crystallized 100 per cent Mg_2SiO_4. Therefore we assume that

the 69-µm astronomical feature is produced by 100 per cent crystalline forsterite. Higher resolution (0.25 cm^{-1}) 3.5- and 295-K measurements presented in Paper I indicated that the decrease in peak-wavelength and width resulted from a difference in temperature between the astronomical and laboratory grains; the shift to shorter wavelengths results from an increase in phonon energy as the lattice contracts, and the features sharpen because a reduction in temperature reduces the phonon density.

2 LABORATORY AND ASTRONOMICAL MEASUREMENTS

Paper I presented laboratory measurements of the effect of temperature on the 69-µm feature of synthetic forsterite, Mg_2SiO_4, powder embedded in petroleum jelly on a polyethylene substrate. Spectra were obtained at 3.5 ± 0.5 and 295 ± 2 K (room temperature). For the new 77^{+5}_{-0} K measurement the same forsterite sample was placed in the output beam of the spectrometer on a liquid nitrogen cooled cold finger. The sampling interval was 0.25 cm^{-1} for each of the measurements. In the current analysis, continua were subtracted from the published data and the wavelength of the 69-µm peak, λ_{pk}, and the full width at half-maximum, $FWHM_{eye}$, were obtained by 'eye' using a cursor because the peaks are asymmetric (see Fig. 1). Ideally the peak shape of the dielectric function at 69 µm is Lorentzian but in practice many laboratory absorption peaks are found to be asymmetric or Gaussian because of a range of particle shapes and sizes (see Paper I). Gaussian fits to the laboratory peaks (dotted lines in Fig. 1) were poor, with high values of χ^2_ν ($\chi^2_\nu \sim 1$ is a good fit) and large residuals (dot–dashed lines) longwards of λ_{pk}. The instrumental FWHM, $FWHM_{inst}$, was 0.5 $cm^{-1} \equiv 0.24$ µm at 69 µm ($= 2 \times$ sampling interval) which is similar to the width of the peak. Therefore the true FWHM, $FWHM_{69\,µm}$, was obtained by subtracting (in quadrature) $FWHM_{inst}$ from $FWHM_{eye}$; λ_{pk} and $FWHM_{69\,µm}$ are shown in Fig. 1.

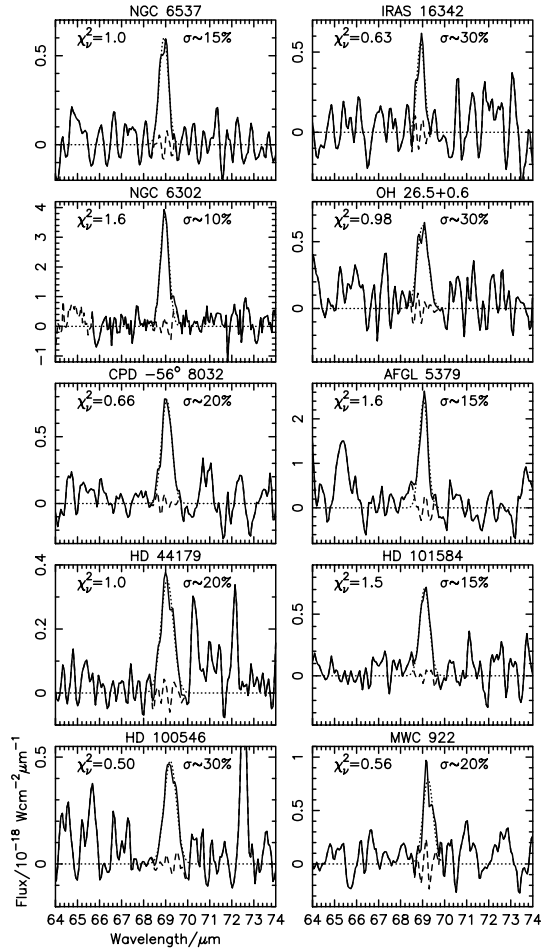Observations of the 69-µm forsterite band were obtained with the LWS on *ISO* (Clegg et al. 1996; Kessler et al. 1996). Data from the ISO archive were reduced with the *ISO* spectral analysis package (ISAP) version 2.0. The target dedicated time (TDT) numbers and exposure times and the version numbers of the online processing packages (OLPs) are listed in Table 1. The 69-µm feature occurs in the overlap region between detectors 3 and 4. Detector 3 is thought to produce more reliable spectral shapes; therefore if data from detector 4 indicated a broader feature, only detector 3 was used to produce the fluxes. Where the agreement between detectors was good the data were merged before averaging
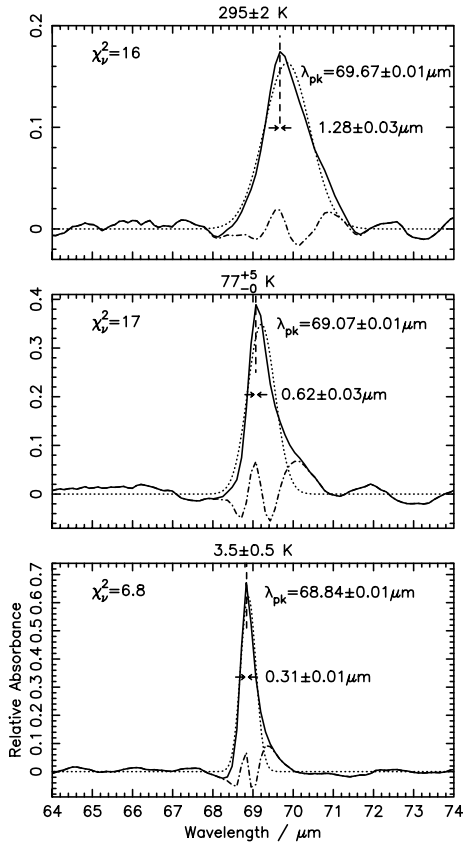
Figure 1. Continuum-subtracted 69-µm laboratory spectra for forsterite at 3.5 ± 0.5, 77^{+5}_{-0} and 295 ± 2 K (solid lines) with Gaussian fits (dotted) and residuals after subtraction of the Gaussians (dot–dashed). Dashed lines indicate λ_{pk} estimated by 'eye'. χ^2_ν is based on $\sigma \sim 1$ per cent of the peak absorbance.

Table 1. Object classifications, target TDT numbers, exposure times, derived values of λ_{pk} and FWHM for the 69-µm feature, for a number of sources where the band has been identified. The penultimate columns lists the estimated grain temperature, $T_{69\,µm}$, derived from λ_{pk} using the laboratory calibration from Paper I. $T_{69\,µm}$ temperature estimates based on Chihara et al.'s (2001) data are 18–24 K higher (see text). The last column lists the temperature of the local continuum, T_{cont}, derived using a dust emissivity index of $\beta = 1.5$.

| Object	Type	TDT	Time/s	OLP	λ_{pk}/µm	FWHM/µm	$T_{69\,µm}$/K	$T_{cont}(\beta = 1.5)$/K
NGC 6537	Planetary nebula	70300625	2230	9.1	68.92 ± 0.02	0.39 ± 0.04	29 ± 6	39 ± 3
IRAS 16342	OH/IR star	08402827	1552	8.7	68.92 ± 0.03	0.29 ± 0.08	27 ± 10	67 ± 12
NGC 6302	Planetary nebula	Many	13243	7.0	68.96 ± 0.02	0.37 ± 0.05	41 ± 6	52 ± 1
OH 26.5+0.6	OH/IR star	33000316	1268	9.5	69.01 ± 0.04	0.52 ± 0.10	57 ± 14	58 ± 9
CPD −56°8032	Planetary nebula	08401538	1552	9.5	69.05 ± 0.02	0.47 ± 0.05	70 ± 7	70 ± 13
AFGL 5379	OH/IR star	46901615	1614	9.1	69.05 ± 0.03	0.37 ± 0.07	69 ± 8	85 ± 17
HD 44179	Red Rectangle	70901203	3428	9.1	69.07 ± 0.05	0.60 ± 0.11	77 ± 16	72 ± 13
HD 101584	Post-AGB object	07901520	1554	9.1	69.09 ± 0.05	0.44 ± 0.06	84 ± 9	64 ± 9
HD 100546	Herbig Ae/Be star	10400640	2228	7.0	69.21 ± 0.05	0.60 ± 0.11	127 ± 18	62 ± 11
MWC 922	Emission-line star	47801237	1316	9.1	69.24 ± 0.03	0.46 ± 0.07	139 ± 10	54 ± 6

Figure 2. Continuum-subtracted LWS observations of the 69-µm forsterite band (solid lines); dotted lines indicate the Gaussian fits used to obtain the wavelength of the peak and the FWHM of the features; dashed lines indicate the residuals obtained after subtraction of the fits. (The estimated uncertainty in the baseline flux, σ, is quoted as a fraction of the peak flux at $\lambda_{69\,\mu m}$.)

to the highest default sampling interval ($\sim 0.066\,\mu m$). NGC 6302 was observed frequently during the *ISO* mission as a calibration source and the included spectrum was originally presented and analysed by Molster et al. (2001). Hence the signal-to-noise ratio for this observation is significantly better than that for the other 69-µm features. To obtain 69-µm features with zero baselines for Gaussian fitting, the data were smoothed with a Gaussian function with FWHM ≈ 2 pixel. Then continua (with no physical significance) were assessed between 63.5 and 80 µm and subtracted from the flux spectra; the residual 69-µm features are shown in Fig. 2. Since Gaussians were a good match to the peaks (see Fig. 2), both the characteristic wavelength λ_{pk} and the FWHM were obtained by fitting Gaussians using the emission-line fitting routine ELF in the Starlink DIPSO spectroscopic analysis package. The instrumental FWHM resolution of the LWS is $0.29\,\mu m$ (Swinyard et al. 1996), and this was subtracted in quadrature to obtain the observed FWHM values listed in Table 1.

3 FORSTERITE 69-µm TEMPERATURES

The derived FWHMs of the astronomical and laboratory 69-µm features, $\mathrm{FWHM}_{69\,\mu m}$, are plotted as a function of the peak wavelength, λ_{pk}, in Fig. 3. To place limits on the effects of experimental artefacts such as grain size, sample density and matrix effects, these values are compared with those from laboratory data by Chihara, Koike & Tsuchiyama (2001); their values were obtained from room-temperature (CRT; we assume 295 ± 5 K) and low-temperature (CLT; ~ 4.2 K; we assume ± 5 K) spectra of a synthetic forsterite sample embedded in polyethylene, at resolutions of 0.5 and $0.1\,\mathrm{cm}^{-1}$, respectively.

Since λ_{pk} and $\mathrm{FWHM}_{69\,\mu m}$ are temperature-dependent, both values should be used to estimate the temperature of the astronomical grains. The astronomical values of λ_{pk} fall within the range of both laboratory data sets. However, the astronomical 69-µm bands are significantly narrower than expected from the laboratory relation between λ_{pk} and FWHM (see Fig. 3). IRAS 16342 has a narrower 69-µm band than our 3.5-K measurement. This, along with baseline uncertainties and laboratory sample
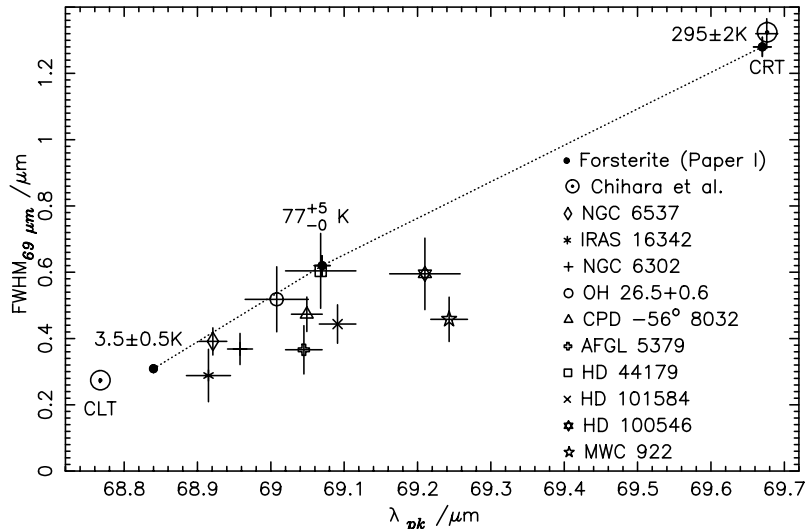
Figure 3. The FWHM of the astronomical and laboratory 69-µm bands ($\mathrm{FWHM}_{69\,\mu m}$) as a function of the peak wavelength of the feature, λ_{pk}. Laboratory data points from Paper I and the 77-K measurement are joined by dotted lines to guide the eye. Low-temperature and room-temperature measurements of forsterite by Chihara et al. (2001) are marked CLT and CRT, respectively. Errors are deduced from the statistics of the Gaussian fits.

density effects, precludes the use of the measured FHWM as a temperature indicator at this time (see Section 3.1).

In Table 1 we have interpolated between the peak wavelengths of the laboratory data from Paper I and our 77-K measurement to estimate the characteristic temperature, $T_{69\,\mu m}$, of the forsterite grains. Comparison between the values of λ_{pk} of the astronomical and laboratory forsterite bands suggests that the astronomical grain populations are in the 27- to 139-K temperature range.

The Chihara et al. values of λ_{pk} differ from ours by 0.01 μm (CRT) and 0.07 μm (CLT) The source of the difference between the values of λ_{pk} is currently unknown. One possibility is the difference between the refractive indices of the petroleum jelly (Paper I) and polyethylene media (Chihara et al.) in which the forsterite powders were embedded. However, we could find no measurements for either material at any temperature or wavelength. Matrix effects in KBr have been investigated by Colangeli et al. (1995) for $\lambda < 30$ μm and by Speck, Hofmeister & Barlow (1999) for 6–20 μm. Colangeli et al. found $0.00 \lesssim |\lambda_{shift}| \lesssim 0.05$ μm, whilst Speck et al. found that shifts were introduced only when grains were sufficiently large to saturate the infrared peaks, i.e. that the shift depended on the grain properties and not on the matrix. Grain temperatures derived by interpolating between the two Chihara et al. reference temperatures would produce a $T_{69\,\mu m}$ that is 18 K higher for the warmer grains surrounding HD 100546 and MWC 922, and 24 K higher for objects with λ_{pk} less than 69.07 μm (the 77-K laboratory peak).

The derivation of grain temperatures by interpolation assumes a linear temperature relation between the measurements. The relationship is imprecise because of an absence of data at intermediate temperatures. Since the wavelength shift of the peak depends on the contraction of the lattice, it is possible that the band shift approaches zero at some temperature above 3.5 K. Forsterite (like the majority of crystalline solids) has constant anisotropic thermal expansion coefficients between 100 and 2000 K (close to its melting point: e.g. Gillet, Daniel & Guyot 1997). However, at temperatures $\lesssim 80$ K ($\sim 0.1 \times$ the Debye temperature of 766 K), the measured coefficients decrease (White, Roberts & Collins 1985) to a limiting value of zero at 0 K. Further measurements of the 69-μm peak at a range of low temperatures, grain sizes and matrix effects are required for better determinations of characteristic grain temperatures.

3.1 Bandwidth variation

The decrease in the FWHM for an individual sample as the

temperature is reduced is due to the decrease in phonon density at low temperatures and the consequent increase in the phonon lifetimes (see Paper I). However, the measured widths depend on the baseline, the grain size distribution, the sample density and the refractive indices of polyethylene or petroleum jelly matrix. Chihara et al. quote FWHMs of 1.34 and 0.27 μm from Lorentzian fits to their room-temperature (CRT) and low-temperature (CLT) measurements, respectively. Their sampling intervals at the two temperatures corresponded to 0.24 μm (CRT) and 0.05 μm (CLT); assuming instrumental resolutions of 2× the sampling interval, their intrinsic FWHMs are 1.32 μm (CRT) and 0.27 μm (CLT), whilst our values are 1.28 μm (295 K) and 0.31 μm (3.5 K). The Chihara FHWM measurements may be nearer the true value since their peaks are probably more symmetric because their grains were < 1 μm in size, whilst the size distribution of our thin films was unconstrained.

The astronomical 69-μm bands are narrower than expected for the laboratory relation between λ_{pk} and FWHM (see Fig. 3). The pre-main-sequence objects MWC 922 and HD 100546 are the most discrepant, having narrower bands with respect to λ_{pk} than the post-main-sequence objects. For the post-main-sequence objects, FWHM increases with λ_{pk}, as expected. The narrowness of the observed astronomical peaks suggests that the forsterite grains may be smaller and/or have a smaller size distribution than the laboratory samples, since in room-temperature laboratory studies the widths of peaks caused by absorption in a single crystal (and hence a single path length) tend to be smaller than data obtained from powders (e.g. Hofmeister et al. 2000). Laboratory measurements of the interplay between sample density, grain size, matrix effects and temperature are required before FWHMs can be used with λ_{pk} to derive reliable estimates of these parameters.

4 COMPARISON WITH LONG-WAVELENGTH CONTINUUM TEMPERATURES

Continuum temperatures were obtained from the unsmoothed ~ 57–83 μm spectra by using the blackbody fit routine in ISAP 2.0 and masking emission features such as the [O I] line at 63.2 μm and the forsterite band. The continua of NGC 6537 and 6302 over this wavelength range are affected by a broad emission feature between 60 and 70 μm (see Molster et al. 2001). Therefore for NGC 6302 the continuum temperature was obtained from the full 50–190 μm spectrum.

The blackbody fitting routine approximates the featureless
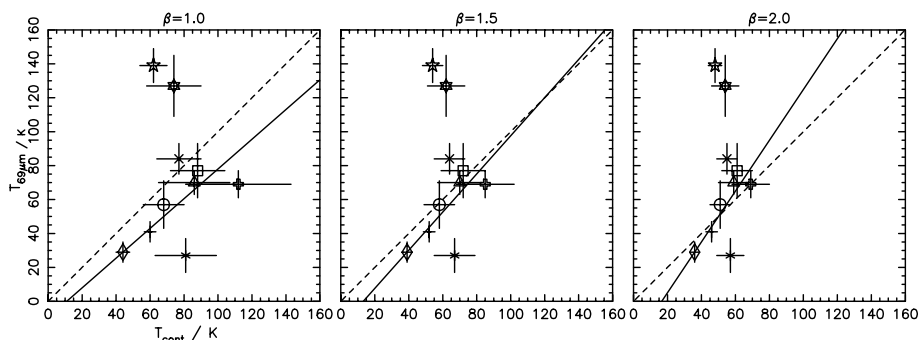
Figure 4. Forsterite 69-μm temperature plotted as a function of continuum temperature. Solid lines denote the weighted fit to objects with forsterite 69-μm temperatures less than 85 K, i.e. excluding the two pre-main-sequence objects. $T_{69\,\mu m} \sim T_{cont}$ when $\beta = 1.5$. For this value of β, $y = (1.1 \pm 0.3)x - (15 \pm 17)$ K.

continuum flux, $F_\lambda \propto B(\lambda, T)\lambda^{-\beta}$, where $B(\lambda, T)$ is the blackbody function and β is the dust emissivity index. The values of T and β cannot be derived independently, owing to warmer dust emitting at shorter wavelengths and a lack of data longwards of $180\,\mu\text{m}$. Single-temperature-component fits to the Galactic spectrum (Wright et al. 1991) gave $\beta = 1.65$ and a dust temperature of $23.3\,\text{K}$, and their two-temperature fits (20.4 and 4.77 K) used $\beta = 2.0$, the value given by the Kramers–Kronig theorem in the low-frequency limit. Since β values are relatively uncertain, we tried values of 1.0, 1.5 and 2.0. The 69-μm forsterite band temperatures, $T_{69\,\mu\text{m}}$, are compared with the resulting continuum temperatures, T_{cont}, in Fig. 4. Dashed lines show where $T_{69\,\mu\text{m}} = T_{\text{cont}}$ and solid lines indicate weighted line fits to the post-main-sequence objects only, which all have 69-μm forsterite band temperatures of less than 85 K. The fits show that increasing the value of β decreases both the continuum temperature and the derived uncertainty, and that $\beta = 1.5$ produces the closest match between the continuum temperature estimates, T_{cont}, and the forsterite 69-μm-peak temperatures, $T_{69\,\mu\text{m}}$.

5 DISCUSSION

5.1 Post-main-sequence versus pre-main-sequence objects

Fig. 4 shows that the derived dust continuum temperatures for the eight post-main-sequence objects matched the forsterite 69-μm-peak temperatures most closely when $\beta = 1.5$. T_{cont} for $\beta = 1.5$ is listed in Table 1 for each of the objects. As discussed above, this suggests that the emission from the post-main-sequence objects is produced by dust with similar emission properties to interstellar dust. The close agreement between the 69-μm and continuum temperatures also indicates that the forsterite grains and 'featureless' dust components are probably spatially related.

For the two pre-main-sequence objects, HD 100546 and MWC 922, the derived $T_{69\,\mu\text{m}}$ temperatures are 127 ± 18 and $139 \pm 10\,\text{K}$, respectively, significantly warmer than their $\beta = 1.5$ continuum temperatures of 62 ± 11 and $54 \pm 6\,\text{K}$. If the objects were surrounded mainly by larger (radius $\gtrsim 20\,\mu\text{m}$) grains, with constant opacity in the ~ 57–$83\,\mu\text{m}$ range (i.e. $\beta = 0.0$), the derived continuum temperatures would rise to 127 ± 53 and $94 \pm 19\,\text{K}$. Hence for HD 100546 the forsterite temperature could be consistent with grain growth, but for MWC 922 the forsterite grains are still $\sim 45\,\text{K}$ warmer than the underlying continuum. The discrepancy between $T_{69\,\mu\text{m}}$ and T_{cont} for MWC 922 and the high forsterite temperature in HD 100546 could suggest that the forsterite 69-μm emission may originate in hotter optically thin layers above an optically thick circumstellar disc or torus. This scenario was also suggested by Bowey & Adamson (2001) to explain the presence of optically thin emission from 'amorphous' silicate dust in the 10-μm spectrum of HL Tau.

5.2 Is the 49-μm forsterite feature present in the *ISO* spectra?

Fig. 5 of Bowey et al. (2001) shows that, in addition to a 69-μm feature, forsterite grains also exhibit a 49-μm feature. For grain temperatures of 295 K, the ratio of the flux in the 49-μm band to the flux in the 69-μm band is 5.4, with the flux ratio declining to 2.3 at 70 K and 0.3 at 27 K. Hence cooler grains are less likely to exhibit an observable 49-μm peak. We have checked whether our LWS spectra are consistent with the strengths expected for the 49-μm forsterite band. To predict the flux of the 49-μm peak for each object, we scaled the 69-μm band profile of NGC 6302 to the flux
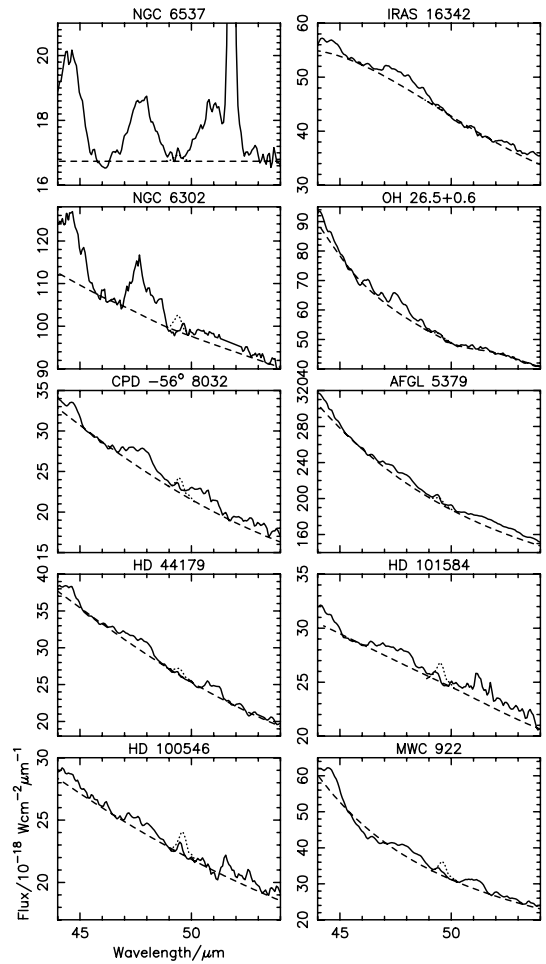
Figure 5. LWS observations of the 49-μm region (solid) with simulated continua (dashed) and the predicted forsterite 49-μm peaks (dotted); see Section 5.2.

level predicted for the 49-μm feature. To estimate this flux level, we multiplied the measured 69-μm band flux of the object by the predicted 49- to 69-μm band-flux ratio at the temperature, $T_{69\,\mu\text{m}}$, derived from the peak wavelength of the 69-μm band. We then added the resulting 49-μm band profile to the observed LWS spectrum at 49 μm to see whether a detectable 49-μm feature should have been present. The results are shown in Fig. 5. We note that, owing to (i) the steep rise in the continuum level of the spectra between 69 and 49 μm which reduces the contrast of shorter wavelength features, and (ii) the higher noise level in LWS Detector 1 which covered the 49-μm region compared with Detector 3 which covered the 69-μm region, it is intrinsically more difficult to detect features at 49 μm than at 69 μm. For NGC 6537, IRAS 16342 and OH 26.5+0.6, the expected 49-μm feature would not have been detectable; for NGC 6302 and HD 101584, the predicted 49-μm features are stronger than the features in the spectra. However, CPD-56° 8032, HD 44179 and AFGL 5379 have observed 49-μm features that are consistent with those predicted. In particular, the object in our sample with the strongest continuum flux, and thus the highest signal-to-noise ratio spectrum, AFGL 5379, is found to have an observed feature at 49 μm that is very consistent in both flux and peak wavelength with that predicted by the combined strength and peak wavelength of its 69-μm band. For the two pre-main-sequence objects, HD 100546 and MWC 922, the

predicted strength of the 49-μm band is significantly higher than the observational upper limits (Fig. 5). However, as noted earlier, for these two objects the temperatures derived from the wavelength of the 69-μm peak, $T_{69\,\mu m}$, are significantly higher than those derived from local continuum fits, and also significantly higher than the temperatures implied by the FHWMs of their 69-μm features. The adoption of lower forsterite temperatures, consistent with either the 69-μm continua fits or the observed 69-μm band FWHMs, would predict considerably weaker strengths for the 49-μm forsterite features for these two objects, consistent with the *ISO* LWS data.

6 CONCLUSIONS

We have compared the peak wavelength and FWHM of the 69-μm astronomical emission feature observed by the LWS on *ISO* with those of the corresponding absorption feature of forsterite measured at 295, 77 and 3.5 K. By interpolating between the laboratory measurements of peak wavelength we deduce characteristic forsterite 69-μm temperatures in the $27-84\,\mathrm{K}$ ($\pm 6-18\,\mathrm{K}$) range for the eight post-main-sequence objects sampled. These values are also found to be consistent with continuum temperatures derived with a grain emissivity index of $\beta = 1.5$. In contrast, the characteristic 69-μm temperatures of forsterite dust surrounding the pre-main-sequence objects HD 100546 and MWC 922 are higher (127 ± 18 and $139 \pm 10\,\mathrm{K}$, respectively) than for the post-main-sequence objects. In the large-particle limit, with $\beta = 0.0$, their respective continuum temperatures are 127 ± 53 and $94 \pm 19\,\mathrm{K}$, which although showing improved agreement with their forsterite 69-μm temperatures may imply that the 69-μm peak is produced by forsterite grains that are spatially separated from the dust responsible for the continuum emission. We have also shown that the strengths predicted for the 49-μm forsterite feature from the 69-μm feature strengths and peak wavelengths are generally consistent with the *ISO* LWS observations. We conclude that observations of the peak wavelength and FWHM of the 69-μm forsterite band show great promise as a new diagnostic of characteristic grain temperatures.

REFERENCES

Bowey J. E., Adamson A. J., 2001, MNRAS, 320, 131
Bowey J. E., Lee C., Tucker C., Hofmeister A. M., Ade P. A. R., Barlow M. J., 2001, MNRAS, 325, 886 (Paper I)
Chihara H., Koike C., Tsuchiyama A., 2001, PASJ, 53, 243
Clegg P. E. et al., 1996, A&A, 315, L38
Colangeli L., Mennella V., diMarino C., Rotundi A., Bussoletti E., 1995, A&A, 293, 927
Gillet P., Daniel I., Guyot F., 1997, Eur. J. Mineral., 9, 255
Hofmeister A. M., 1997, Phys. Chem. Mineral., 24, 535
Hofmeister A. M., Keppel E., Bowey J. E., Speck A. K., 2000, in Salama A., Kessler M. F., Leech K., Schulz B., eds, ESA SP-456, *ISO* beyond the peaks: the second *ISO* workshop on analytical spectroscopy. ESA, Noordwijk, p. 343
Kessler M. F. et al., 1996, A&A, 315, L27
Koike C., Shibai H., Tuchiyama A., 1993, MNRAS, 264, 654
Malfait K., Waelkens C., Waters L. B. F. M., Vandenbussche B., Huygen E., de Graauw M. S., 1998, A&A, 332, L25
Molster F. J. et al., 2001, A&A, 372, L165
Speck A. K., Hofmeister A. M., Barlow M. J., 1999, ApJ, 513, L87
Swinyard B. M. et al., 1996, A&A, 315, L43
Waelkens C. et al., 1996, A&A, 315, L245
White G. K., Roberts R. B., Collins J. G., 1985, High Temp. High Press., 17, 61
Wright E. L. et al., 1991, ApJ, 381, 200

This paper has been typeset from a TEX/LATEX file prepared by the author.